RESEARCH ARTICLE | JUNE 21 2022

Improved moisture resistance and interfacial recombination of perovskite solar cells by doping oleylamine in spiro-OMeTAD based hole-transport layer ⊘



Appl. Phys. Lett. 120, 253503 (2022) https://doi.org/10.1063/5.0092110

A CHORUS





Citation

CrossMark

Articles You May Be Interested In

Direct observation of dramatically enhanced hole formation in a perovskite-solar-cell material spiro-OMeTAD by Li-TFSI doping

Appl. Phys. Lett. (March 2017)

Insights into the hole transport properties of LiTFSI-doped spiro-OMeTAD films through impedance spectroscopy

J. Appl. Phys. (August 2020)

Electronic structure of the clean interface between single crystal $\text{CH}_3\text{NH}_3\text{PbI}_3$ and an organic hole transporting material spiro-OMeTAD

Appl. Phys. Lett. (June 2020)

500 kHz or 8.5 GHz? And all the ranges in between.

Lock-in Amplifiers for your periodic signal measurement









Improved moisture resistance and interfacial recombination of perovskite solar cells by doping oleylamine in spiro-OMeTAD based hole-transport layer

Cite as: Appl. Phys. Lett. **120**, 253503 (2022); doi: 10.1063/5.0092110 Submitted: 21 March 2022 · Accepted: 9 June 2022 · Published Online: 21 June 2022







Shan Liu,¹ Shuyue Wu,¹ Pufeihong Xia,¹ Haipeng Xie,¹ [p Xiaoming Yuan,¹ [p Youzhen Li,¹ [p Deming Kong,¹ Han Huang,¹ [p Yongli Gao,² [p and Conghua Zhou¹.a¹ [p

AFFILIATIONS

¹Hunan Key Laboratory of Super-microstructure and Ultrafast Process in Advanced Materials, Hunan Key Laboratory of Nanophotonics and Devices, School of Physics and Electronics, Central South University, Changsha, Hunan 410083, People's Republic of China

ABSTRACT

Hydrophobic and long-chain molecule oleylamine is used to modify the spiro-OMeTAD matrix, which is then adopted for the hole-transport layer in perovskite solar cells. It is observed that after moderate doping, the power conversion efficiency of the devices increases from 17.82 (± 1.47)% to 20.68 (± 0.77)%, with the optimized efficiency of 21.57% (AM 1.5G, 100 mW/cm²). The improved efficiency is ascribed to the favored charge extraction and retarded charge recombination, as reflected by transient photovoltage/photocurrent curves and impedance spectroscopy measurement. In addition, the grazing incidence photoluminescence spectrum reveals that oleylamine doping causes a blue shift of the luminescence peak of the surface layer of the halide perovskite film, while the Mott—Schottky study observes 100 mV increment in the built-in potential, both of which indicate possible defect passivation behavior on the perovskite. Moreover, an accelerated damp test observes that moisture resistance of the device is also upgraded, which is due to the improved hydrophobicity of the spiro-OMeTAD matrix.

Published under an exclusive license by AIP Publishing. https://doi.org/10.1063/5.0092110

Over the past decade, fast development has been witnessed in the organic-inorganic halide perovskite solar cells (PSCs), leading to the certified power conversion efficiency (PCE) of 25.7%, compared to pioneered 3.81% in 2009.2 Such performance is quite appealing for mass applications, though balance between "efficiency-cost-stability" or the so-called Golden triangles should be well dealt with.^{3,4} As long as the top electrode is concerned, two kinds of PSCs have been widely studied: those based on metal- or on carbon-electrode. Usually, carbon-electrode based devices are known by the "hole-conductorfree" feature. 5,6 They have shown excellent stability due to the pristine inert nature and penetration resistance against moisture and oxygen (H2O/O2) of the carbon-electrode, though the efficiency is relatively low due to poor interface between the electrode and photo-active layer. 7,8 Anyhow, adding one more layer of hole-conductor (or holetransport layer, HTL in short) to the interface is seen as helpful for power conversion.^{9,10} As for metal-electrode devices, they have shown

the highest efficiencies due to suitable energy band alignment, though suffer from stability problems that arise from corrosion of the top electrode by the organic-inorganic halide perovskite material, 11-14 and the H₂O/O₂ penetration through the top electrode. ^{15–20} In fact, such penetration could easily happen in thin-film devices. To reduce the cost, the top metal film is usually $0.1 \, \mu m$ in thickness; in addition, the charge-transport layer beneath the top electrode is also $\sim 0.1 \,\mu\text{m}$. Such a feature could hardly prevent the H₂O/O₂ penetration. What is more, sometimes poor film quality is observed for the charge-transport layer under the top electrode. For example, for the famous 2,2',7,7'-tetrakis [N, N-di (4-methoxyphenyl) amino]-9,9'-spiro-bifluorene (spiro-OMeTAD), which is known as an ideal HTL material due to the matching of valence band energy between it and the halide perovskite and high carrier mobility $(10^{-3}-10^{-4} \text{ cm}^2/\text{V s})$. However, it usually comes out with a porous structure, as revealed by Qi and coworkers. This accelerates the H₂O/O₂ penetration and, thus, the decomposition

 $^{^2}$ Department of Physics and Astronomy, University of Rochester, Rochester, New York 14627, USA

a) Author to whom correspondence should be addressed: chzhou@csu.edu.cn

of the active layer. To solve this problem, the film quality of this HTL layer must be improved. For example, adding a PMMA polymer was found to improve the continuity and the compactness of the HTL matrix and, hence, the device stability, due to the improved barrier for " $H_2O/O_2/Ag$ ". ^{23,24} In addition, Han *et al.* inserted a chlorinated grapheneoxide (Cl-GO) layer into the interface between "perovskite/PTAA", also reduced the decomposition risk. ²⁵ Consequently, the high quality HTL is a necessity to upgrade both efficiency and stability of PSCs. Honestly, halide perovskite is very sensitive to moisture. Carbon-electrode devices usually own high moisture resistance due the usage of μ m-thick carbon film on top. Similarly, the moisture resistance of metal-electrode devices should also be upgraded, possibly by increasing the compactness and hydrophobicity of layers on top of the active layer. ²³

Amine group (-NH2) containing molecule, a molecule, such as oleylamine (OA), ²⁶ hexylamine (HA), ²⁷ dodecylamine hydroiodide (DAHI), ²⁸ and bilateral alkylamine (BAA), ²⁹ has been imported to passivate defects in a perovskite film due to the possible interaction between them. Due to the hydrophobicity owned by these molecules, moisture resistance of devices was usually improved. Among these molecules, OA weighs the highest due to the longest carbon chain it has. Such a feature would be of interest when considering the merit in film formation. As such, here in this work, following previous PMMA doping, OA is added to the spiro-OMeTAD based HTL matrix. As will be seen later, OA modification not only improves the moisture resistance, but also upgrades the device efficiency.

As shown in the inset of Fig. 1(a), PSCs with the device structure of FTO/SnO₂/perovskite/spiro-OMeTAD@OA/Ag are prepared, following

the method described before.²³ According to experiment, the chemical formula of perovskite could be noted as "FAxMA(1-x)Pb(IvBr1-v)3," or noted by PVSK in the following description. Typical procedures, information of materials and reagents, and the characterization methods are all included in the supplementary material. Noting that, OA (C₁₈H₃₇N) holds molecule chain of 18 carbon atoms with an amide group (-NH₂) at the end, which is shown in the inset of Fig. 1(a). To study the effect brought by OA, certain volume of OA was added to the spiro-OMeTAD solution matrix, or 0 (reference), 15, 30, 50, and 80 μ l, respectively. Concentration of spiro-OMeTAD and other additives are kept the same. Adding OA in the spiro-OMeTAD basing HTL matrix could bring two aspects of merits on PSCs or power conversion and moisture resistance. For detailed comparison, statics are carried out on the performance parameters. Typical current density-voltage curves are shown in Fig. 1(a), indicating that OA doping could upgrade the performance parameters, like open-circuit voltage (V_{OC}), short-circuit current density (J_{SC}), fill factor (FF), and power conversion efficiency (PCE). These parameters are shown in Figs. 1(b), 1(c), 1(e), and 1(f), respectively. As for V_{OC}, it rises from 0.97 (\pm 0.03) V (reference devices) to 1.06 (\pm 0.02)V (30 μ l OA added), while FF increases from 73.66 (±3.62) % to 78.83 (± 1.18)%. Increment of 9.28% and 7.01% was resolved for V_{OC} and FF, respectively. Moreover, J_{SC} changes slightly, increasing from 24.53 (± 0.52) to 24.69 (± 0.44) mA/cm². Due to the contribution of V_{OC} and FF, PCE raises from 17.82 (±1.47)% (reference devices) to 20.68 $(\pm 0.77)\%$ (30 μ l OA added), increasing by 16.05%. Noting that, Fig. 1(a) shows two typical JV curves from reference device (0 μ l OA added) and modified device (30 μ l). The corresponding performance parameters

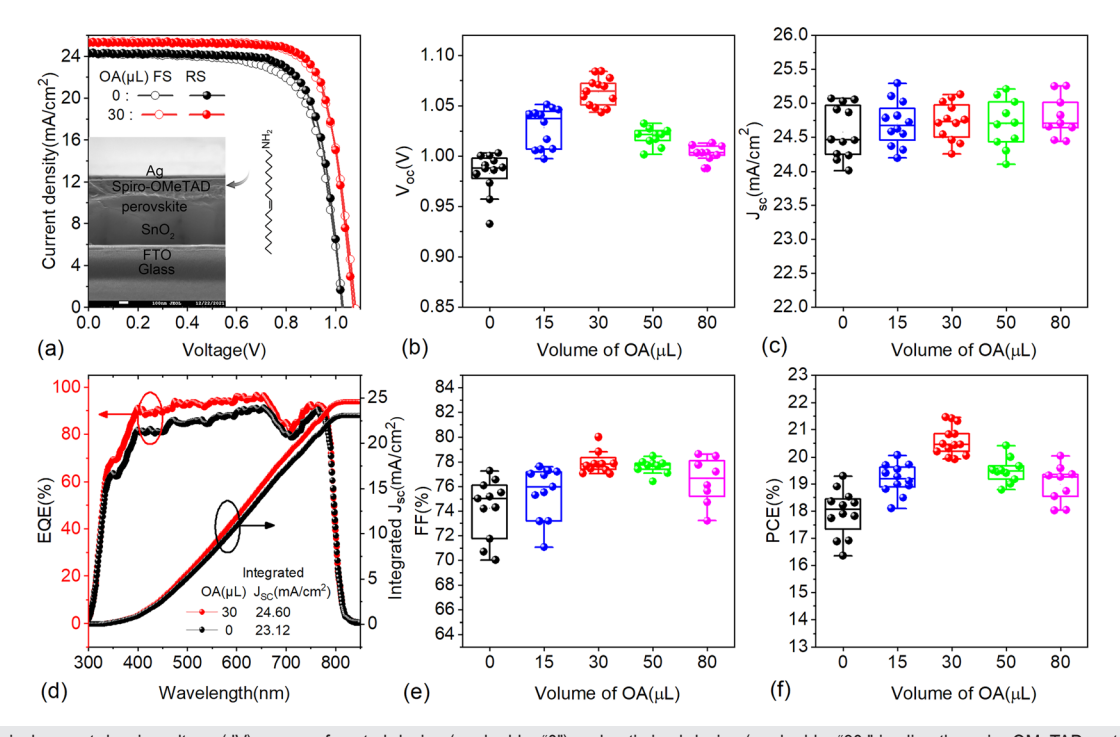


FIG. 1. (a) Typical current densiy–voltage (JV) curves of control device (marked by "0") and optimized device (marked by "30," impling the spiro-OMeTAD matrix is doped by 30 μ l OA). The JV curves are measured at simulated illumination (AM 1.5G, 100 mW/cm²), and "FS/RS" represents forward/reverse scans, respectively. The effect of OA doping on the performance parameters: (b) V_{OC} , (c) J_{SC} , (e) FF, and (f) PCE. (d) Typical external quantum efficiency curves and integrated J_{SC} of control/optimized devices. Inset of (a) shows cross-sectional SEM image of a typical device.

(reverse scan or "RS" mode) are $1.07\,\mathrm{V}$ ($\mathrm{V_{OC}}$), $76.92\%(\mathrm{FF})$, $25.3\,\mathrm{mA/cm^2}$ ($\mathrm{J_{SC}}$), and 20.8% (PCE) for the OA-modified device ($30\,\mu\mathrm{l}$), compared to $1.03\,\mathrm{V}(\mathrm{V_{OC}})$, 74.38% (FF), $24.23\,\mathrm{mA/cm^2}$ ($\mathrm{J_{SC}}$), and 18.5% (PCE) for reference device. External quantum effificiency (EQE) is tested, and $\mathrm{J_{SC}}$ is integrated according to illumination spectrum (AM1.5G, $100\,\mathrm{mW/cm^2}$). The result is shown in Fig. 1(d), indicating 24.6 and $23.12\,\mathrm{mA/cm^2}$, corresponding to 97.2% and 95.4% of the reference and OA-modified devices, respectively. EQE curves and corresponding JV curves of modified devices (with other volumes) are shown in Figs. S1(a) and S1(b), respectively. A champion efficiency of 21.57% is achieved, with corresponding JV curve as shown in Fig. S2. In addition, statistics on hysteresis index is performed, as shown in Fig. S3. As expected, relatively low hysteresis index is obtained for OA-modified devices, especially for the case of $30\,\mu\mathrm{l}$.

The improved device performance is ascribed to the retarded carrier recombination and the enhanced charge extraction. Transient photovoltage/photocurrent (TPV/TPC) decay curves are performed on the devices. Typical curves are shown in Fig. S4, while the lifetime (τ) and charge transition time (t_d) are fitted from the TPV/TPC decay curves, respectively. All of these four parameters are presented in Figs. 2(a) and 2(b). It could be seen that lifetime (τ) is 12.94 (\pm 1.5) μ s for reference devices, while nearly doubled to 23.03 (\pm 3.5) μ s when 30 μ l OA was added in the HTL, showing that the recombination is efficiently reduced. As for charge transition time (t_d), it is 3.54(\pm 1.4) μ s for reference devices, while drops slowly to 1.54 (\pm 0.3) μ s where 30 μ l OA is added, showing that the extraction is slightly acceletrated. Comparing to the performance parameters shown in Fig. 1 could see

that V_{OC} evolves in parallel with τ , while J_{SC} moves in contrast (slightly) to t_d. Honestly, such phenomenon was observed several times in previous studies, indicating close relationship between these parameters. 23,30-33 In more, it could also be seen that the FF in Fig. 1(e) also moves in parallel with V_{OC}. Thus, the retarded recombination might also contribute to the elevated FF. 23,34,35 Impedance spectra (IS) show similar results. Typical Nyquist plots are shown in Fig. S5, charge recombination resistance (R_{rec}) and charge transfer resistance (R_{ct}) are picked from simulation on these plots, and the results are shown in Figs. 2(d) and 2(e). R_{rec} is 0.48 (± 0.25) \times 10 $^7\Omega$ for reference devices, increasing to 6.83 (± 1.37) \times 10⁷ Ω for 30 μ l-OA doped devices. While for R_{cb} it is 3.11 (± 0.75) $\times 10^4 \Omega$ for reference devices, being reduced to 1.31 (± 0.27) × $10^4 \Omega$ for 30 μ l-OA modified devices. In addition, comparison between Figs. 2(a) and 2(d), Figs. 2(b) and 2(e) could find similar trends among each pair, showing close relationship between TPV/TPC and IS studies.²³ As a result, the improvement is ascribed to retarded recombination, and the accelerated charge extraction. The retarded recombination is due to the passivation on interfacial defects. Mott-Schottky study [Fig. 2(c)] observes that OA modification brings larger built-in potential (Vbi). For example, it is $0.87 \,\mathrm{V}$ for the reference device, while rising to $0.97 \,\mathrm{V}$ after 30 μl OA is added. Grazing photoluminascence (PL) is used to judge the possible passivation behaivor. As shown in inset of Fig. 2(f), the incident laser is guided to the surface of pervoskite with a small angle ($\sim 10^{\circ}$), by which PL information on the surface layer could be clearly distinguished. It can be been that, bare FA basing perovskite film shows PL peak at 804 nm, it shifts negatively to 800 nm after the perovskite film is modified by thin layer of PMMA, to 798 nm after the perovskite

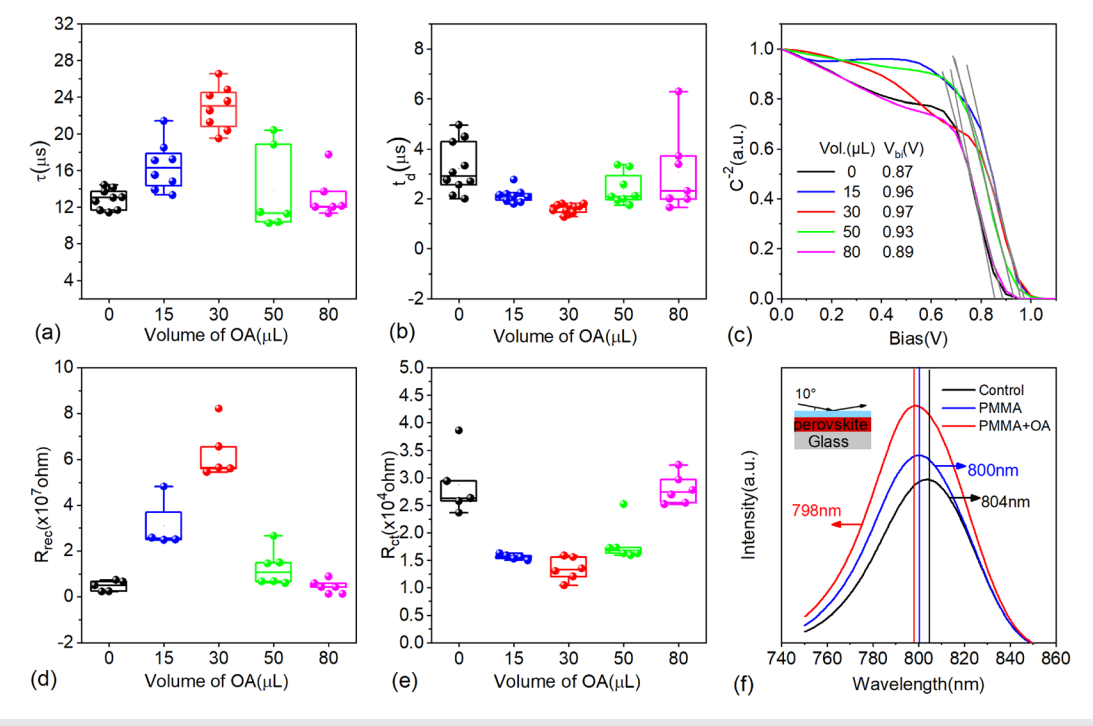


FIG. 2. Effect of OA modification on: (a) lifetime (τ) , (b) transition time (t_d) , (c) Mott—Schottky testing curves, (d) recombination resistance (R_{re}) , and (e) charge transfer resistance (R_{ct}) of PSCs. (f) Grazing photoluminescence study on semi-devices. Luminescence spectra of perovskite (from the top) and perovskite modified with PMMA and PMMA/OA are shown in (f), along with the detecting schematic figure.

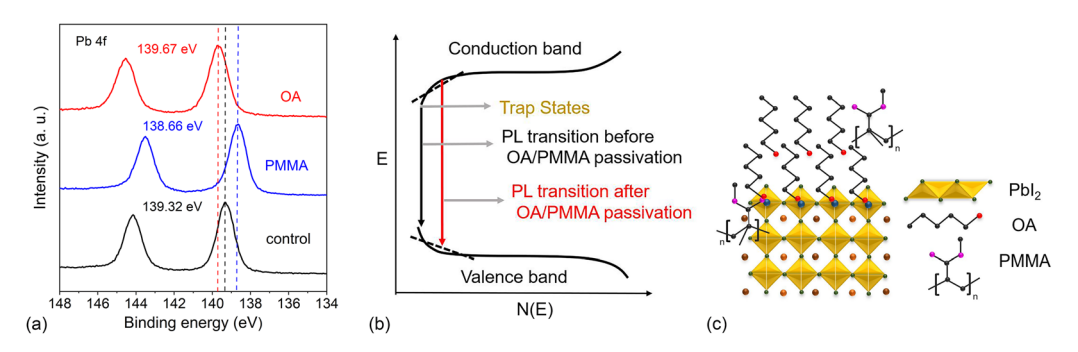


FIG. 3. (a) X-ray Photoelectron Spectroscopy (XPS) of the perovskite film that is modified by PMMA or OA. (b) Schematic diagram of PL after defect passivation. (c) Schematic for the passivation behavior of PMMA/OA on perovskite.

film was modified by both PMMA and OA. For comparison, the effect of OA modification on PL of perovskite is also performed. As shown in Fig. S6(a), negative shift is also observed. Indeed, similar phenomenon was previously reported by Shao *et al.* in 2014.³⁶ The negative shift is due to the reduced defects that lying in the bandgap, as shown schematically in Fig. 3(b). The passivation behavior is due to the interaction between PMMA, OA molecule, and the PVSK crystallite, as will be discussed later. To further confirm the passivation behavior, effect of annealing time on the PL shift is studied. As is shown in Fig. S6(b), with annealing time increasing from 5 to 30 min, PL peak moves from 797.2 to 796 nm. Also, when the laser was guided from the bottom side of the perovskite, the longer luminescence wavelength (800 nm) was observed, compared to 797.2 nm when the laser was guided from the top. These results show that passivation has been achieved on the top surface perovskite layer.

The interaction is examined by x-ray photoelectron spectrum (XPS). As shown in Fig. 3(a), before modification, the binding energy of Pb 4f is 139.32 eV in the pristine PVSK film. After being modified by PMMA, it moves negatively to 138.66 eV, while moves positively to 139.67 eV after modified by OA. In fact, the negative shift is similar to studies, where PMMA was used to modify the quasi-2D Ruddlesden-Popper (RP) perovskite,³⁷ or PMMA contained 3D star-polymer was adopted to modify FA basing PVSK.³⁸ Both of the two works pointed out the possbile coordination behavior between C = O group and the Pb (atom or ion). As such, the negative shift might relate to the such interaction. While for the positive shift in the case of OA, it is similar to that observed in the literature, 26 showing possible interaction between the -NH₂ group and Pb. Due to the possible interaction between PMMA/OA and perovskite, passivation could be harvested, which reduces the defect due to the dangling bond [as shown in Fig. 3(c)] and also retards interfacial recombination and favors the charge transfer. However, more studies are needed to show the cause of the opposite direction shift by these two materials.

To show the improved moisture resistance of devices by OA doping, accelerated aging test was performed by putting devices in an oven, where the relative humidity (RH) could be controlled. As shown in Fig. 4, the devices are treated in RH of 50%, 60%, 70%, 80%, and 85% each for 1 h, and then, the PCE is tested. It can be seen that when there is no OA added, 1 of the 7 starting devices happened to break down after being treated at RH of 60% for 1 h. When 15 µl OA is added, the first breakdown comes out to the treatment at RH of 70% for 1 h. Then, after more OA is added, the breakdown comes later to

RH of 80%. After being treated by RH of 85% for 1 h, 6 of the 7 devices are damaged by moisture in the reference case (no OA added), while only 2 are damaged when 80 μ l OA is added. The breakdown could also be reflected by the optical images that listed in Fig. S7. Clearly, slower decline is seen when HTL is modified by OA. Thus, OA addition elevates the moisture resistance of PSCs. X-ray diffraction (XRD) study is performed on the devices after the accelerated aging test. As shown in Figs. 5(f) and 5(g), the breakdown of devices is accompanied by the decomposition of the perovskite film. After aging test, more PbI₂ and yellow phased perovskite are obtained for reference devices. In more, AgI is observed [Fig. 5(h)] due to the reaction between top Ag electrode and the by-product of perovskite decomposition. 23,39,40 Moreover, storage stability was also recorded, as shown in Fig. S8. One can see that OA modification also improves the storage stability.

To learn more about the effect of OA in above observations, atom force microscopy (AFM) and wettability test were performed on the HTL, as shown in Figs. 5(a)-5(e). It can be seen that OA

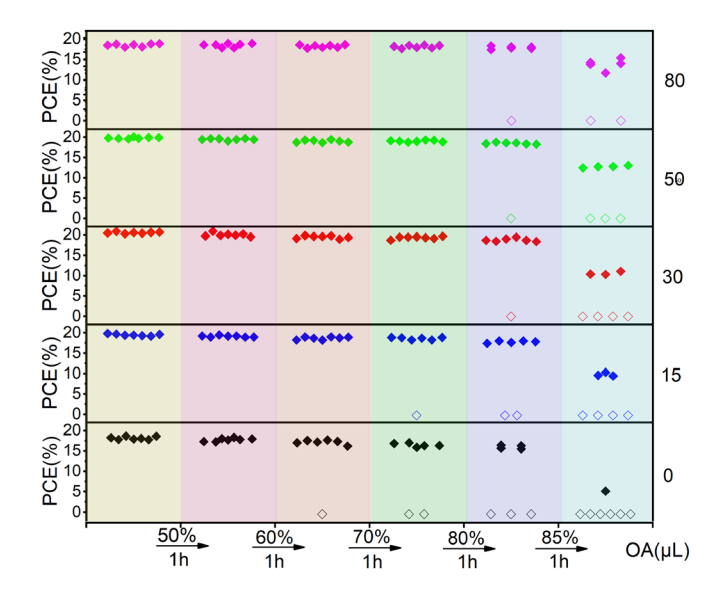


FIG. 4. Accelerated aging test in damp environment. Devices are treated in different moisture environment for 1 h, and then, power conversion efficiency is evaluated. The relative humidity of 50%, 60%, 70%, 80%, and 85% is chosen.

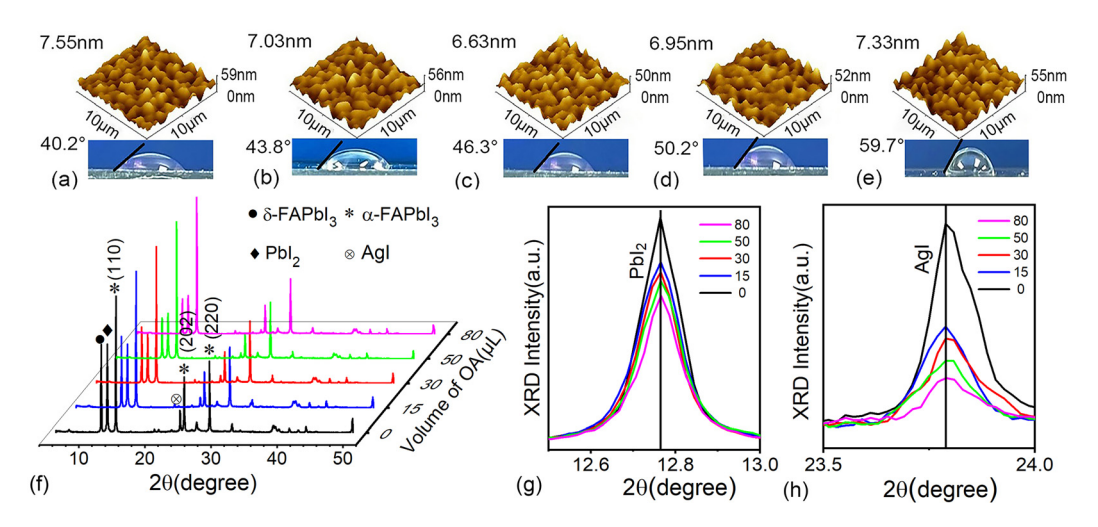


FIG. 5. Effect of OA on surface morphological properties (characterized by atom force microscope) and wettability of spiro-OMeTAD basing HTL (μ I): (a) 0, (b) 15, (c) 30, (d) 50, and (e) 80. (f) XRD diffraction peak of full devices after accelerated aging experiment. (g) and (h) are enlarged part of the XRD spectra at 2θ of 12.8° (for PbI₂) and 23.8° (for AgI), respectively. All of the spectra have been normalized to the peak of (110) of perovskite at each separate spectrum.

modification reduces surface roughness of the HTL, which favors the contact between HTL and beneath perovskite film, and hence, the defects passivation, which benefits device efficiency. On the other hand, OA modification increases the contact angle between water and HTL, showing that more hydrophobic surface is obtained, which helps to raise the moisture resistance. In addition, scanning electron microscope was used to judge the surface morphological properties. As shown in Fig. S9, many pin-holes are seen in bare spiro-OMeTAD films, ^{41,42} which is similar to that reported before. After being modified by PMMA or OA, less pin-holes are observed. As such, PMMA/OA doping is helpful for the film formation process.

In conclusion, due to the interaction between the OA molecule and the perovskite crystallites, passivation behavior is observed, which improves interfacial charge transfer and retards charge recombination and, hence, the power conversion efficiency. Meanwhile, due to the hydrophobicity of OA molecules, doping spiro-OMeTAD based HTL with OA also enhances the moisture resistance of the PSCs. As such, OA could help to prepare a high quality HTL, which is favorable for both efficiency and stability.

See the supplementary material for information about the preparation procedures, materials and reagents, and the characterization methods, EQE, and typical current density-voltage curves corresponding to EQE (Fig. S1), typical JV curves (Fig. S2), statistics on hysteresis index (Fig. S3), typical TPV/TPC curves (Fig. S4), Nyquist plots (Fig. S5), effect of OA modification, annealing and incident direction of laser on PL spectrum of perovskite (Fig. S6), optical images of PSCs (Fig. S7) after accelerated aging test, long-term stability test of PSCs (Fig. S8), and FE-SEM top surface images of the spiro-OMeTAD HTL coated on perovskite film where the HTL is modified by PMMA, OA, or both (Fig. S9).

C. Zhou thanks the financial support of National Natural Science Foundation of China (NSFC, No. 61774170) and Natural Science Foundation of Hunan Province (No. 2020JJ4759). Y. Gao

acknowledges the support from the National Science Foundation, USA (NSF, No. DMR-1903962). S. Liu acknowledges support from the Fundamental Research Funds for the Central South University (No. 2021zzts0502).

AUTHOR DECLARATIONS

Conflict of Interest

The authors have no conflicts to disclose.

DATA AVAILABILITY

The data that support the findings of this study are available within the article and its supplementary material.

REFERENCES

¹See https://www.nrel.gov/pv/assets/pdfs/best-research-cell-efficiencies-rev211214. pdf for PCE records of typical solar cells.

²A. Kojima, K. Teshima, Y. Shirai, and T. Miyasaka, J. Am. Chem. Soc. **131**(17), 6050 (2009).

³L. Meng, J. You, and Y. Yang, Nat. Commun. 9(1), 5265 (2018).

⁴M. Cai, Y. Wu, H. Chen, X. Yang, Y. Qiang, and L. Han, Adv. Sci. 4(1), 1600269 (2017).

⁵Y. Rong, Y. Hu, A. Mei, H. Tan, M. I. Saidaminov, S. I. Seok, M. D. McGehee, E. H. Sargent, and H. Han, Science 361(6408), 1214 (2018).

⁶A. Mei, X. Li, L. Liu, Z. Ku, T. Liu, Y. Rong, M. Xu, M. Hu, J. Chen, Y. Yang, M. Grätzel, and H. Han, Science 345(6194), 295 (2014).

⁷Y. Hu, S. Si, A. Mei, Y. Rong, H. Liu, X. Li, and H. Han, Sol. RRL 1(2), 1600019 (2017).

⁸C. Zhou and S. Lin, Sol. RRL 4(2), 1900190 (2020).

⁹H. Zhang, J. Xiao, J. Shi, H. Su, Y. Luo, D. Li, H. Wu, Y. B. Cheng, and Q. Meng, Adv. Funct. Mater. 28(39), 1802985 (2018).

¹⁰C. Zhang, S. Liang, W. Liu, F. T. Eickemeyer, X. Cai, K. Zhou, J. Bian, H. Zhu, C. Zhu, N. Wang, Z. Wang, J. Zhang, Y. Wang, J. Hu, H. Ma, C. Xin, S. M. Zakeeruddin, M. Graetzel, and Y. Shi, Nat. Energy 6(12), 1154 (2021).

¹¹H. Min, D. Lee, J. Kim, G. Kim, K. S. Lee, J. Kim, M. J. Paik, Y. K. Kim, K. S. Kim, M. G. Kim, T. J. Shin, and S. l. Seok, Nature 598(7881), 444 (2021).

¹²Z. Ni, C. Bao, Y. Liu, Q. Jiang, W. Q. Wu, S. Chen, X. Dai, B. Chen, B. Hartweg, Z. Yu, Z. Holman, and J. Huang, Science 367(6484), 1352 (2020).

- ¹³S. Xiang, W. Li, Y. Wei, J. Liu, H. Liu, L. Zhu, S. Yang, and H. Chen, iScience 15, 156 (2019).
- ¹⁴W. Hui, L. Chao, H. Lu, F. Xia, Q. Wei, Z. Su, T. Niu, L. Tao, B. Du, D. Li, Y. Wang, H. Dong, S. Zuo, B. Li, W. Shi, X. Ran, P. Li, H. Zhang, Z. Wu, C. Ran, L. Song, G. Xing, X. Gao, J. Zhang, Y. Xia, Y. Chen, and W. Huang, Science 371(6536), 1359 (2021).
- ¹⁵B. W. Park and S. I. Seok, Adv. Mater. **31**(20), 1805337 (2019).
- ¹⁶R. Wang, M. Mujahid, Y. Duan, Z.-K. Wang, J. Xue, and Y. Yang, Adv. Funct. Mater. 29(47), 1808843 (2019).
- ¹⁷S. Kundu and T. L. Kelly, EcoMat 2(2), e12025 (2020).
- ¹⁸F. Matteocci, Y. Busby, J.-J. Pireaux, G. Divitini, S. Cacovich, C. Ducati, and A. Di Carlo, ACS Appl. Mater. Interfaces 7(47), 26176 (2015).
- ¹⁹S. Cacovich, L. Ciná, F. Matteocci, G. Divitini, P. A. Midgley, A. D. Carlo, and C. Ducati, Nanoscale 9(14), 4700 (2017).
- ²⁰F. Matteocci, L. Cinà, E. Lamanna, S. Cacovich, G. Divitini, P. A. Midgley, C. Ducati, and A. D. Carlo, Nano Energy 30, 162 (2016).
- N. Ahn, D. Y. Son, I. H. Jang, S. M. Kang, M. Choi, and N. G. Park, J. Am. Chem. Soc. 137(27), 8696 (2015).
- ²²L. K. Ono, S. R. Raga, M. Remeika, A. J. Winchester, A. Gabe, and Y. Qi, J. Mater. Chem. A 3(30), 15451 (2015).
- ²³P. Xia, D. Guo, S. Lin, S. Liu, H. Huang, D. Kong, Y. Gao, W. Zhang, Y. Hu, and C. Zhou, Sol. RRL 5(11), 2100408 (2021).
- ²⁴S. H. Ma, S. Z. Pang, H. Dong, X. P. Xie, G. Liu, P. Dong, D. W. Liu, W. D. Zhu, H. Xi, D. Z. Chen, C. F. Zhang, and Y. Hao, Polymers 14(2), 343 (2022).
- 25Y. Wang, T. Wu, J. Barbaud, W. Kong, D. Cui, H. Chen, X. Yang, and L. Han, Science 365(6454), 687 (2019).
- 26W. Q. Wu, J. X. Zhong, J. F. Liao, C. Zhang, Y. Zhou, W. Feng, L. Ding, L. Wang, and D. B. Kuang, Nano Energy 75, 104929 (2020).
- ²⁷W. Feng, C. Zhang, J. X. Zhong, L. Ding, and W. Q. Wu, Chem. Commun. 56(37), 5006 (2020).

- 28 Y. Zhang, M. Rong, X. Yan, X. Wang, Y. Chen, X. Li, and R. Zhu, Langmuir 34(32), 9507 (2018).
- 29W. Q. Wu, Z. Yang, P. N. Rudd, Y. Shao, X. Dai, H. Wei, Y. Fang, J. Zhao, Q. Wang, Y. Liu, Y. Deng, X. Xiao, Y. Feng, and J. Huang, Sci. Adv. 5(3), eaav8925 (2019).
- ³⁰H. Chen, K. Li, H. Liu, Y. Gao, Y. Yuan, B. Yang, and C. Zhou, Org. Electron. 61, 119 (2018).
- ³¹J. Yan, S. Lin, X. Qiu, H. Chen, K. Li, Y. Yuan, M. Long, B. Yang, Y. Gao, and C. Zhou, Appl. Phys. Lett. 114(10), 103503 (2019).
- ³²T. Shi, S. Lin, M. Fang, D. Kong, Y. Yuan, Y. Gao, B. Yang, H. Han, and C. Zhou, Appl. Phys. Lett. **117**(16), 163501 (2020).
- ³³M. Zhang, M. Ye, W. Wang, C. Ma, S. Wang, Q. Liu, T. Lian, J. Huang, and Z. Lin, Adv. Mater. 32(28), e2000999 (2020).
- 34J. K. Tan, R. Q. Png, C. Zhao, and P. K. H. Ho, Nat. Commun. 9(1), 3269 (2018)
- 35Y. Zeng, D. Li, Z. Xiao, H. Wu, Z. Chen, T. Hao, S. Xiong, Z. Ma, H. Zhu, L. Ding, and Q. Bao, Adv. Energy Mater. 11(31), 2101338 (2021).
- 36Y. Shao, Z. Xiao, C. Bi, Y. Yuan, and J. Huang, Nat. Commun. 5, 5784 (2014).
- ³⁷Q. Cao, J. Yang, T. Wang, Y. Li, X. Pu, J. Zhao, Y. Zhang, H. Zhou, X. Li, and X. Li, Energy Environ. Sci. 14(10), 5406 (2021).
- 38Yukta, M. K. Chini, R. Ranjan, and S. Satapathi, ACS Appl. Electron. Mater. 3(4), 1572 (2021).
- ³⁹T. Leijtens, G. E. Eperon, S. Pathak, A. Abate, M. M. Lee, and H. J. Snaith, Nat. Commun. 4, 2885 (2013).
- ⁴⁰Y. Kato, L. K. Ono, M. V. Lee, S. Wang, S. R. Raga, and Y. Qi, Adv. Mater. Interfaces. 2(13), 1500195 (2015).
- ⁴¹R. Zhao, L. Xie, R. Zhuang, T. Wu, R. Zhao, L. Wang, L. Sun, and Y. Hua, ACS Energy Lett. 6(12), 4209 (2021).
- ⁴²Z. Hawash, L. K. Ono, and Y. Qi, Adv. Mater. Interfaces 5(1), 1700623 (2017).